Topologically Protected Conduction State at Carbon Foam Surfaces: An *Ab initio* Study

Zhen Zhu, Zacharias G. Fthenakis, Jie Guan, and David Tománek*
Physics and Astronomy Department, Michigan State University, East Lansing, Michigan 48824, USA
(Received 22 August 2013; published 14 January 2014)

We report results of *ab initio* electronic structure and quantum conductance calculations indicating the emergence of conduction at the surface of semiconducting carbon foams. The occurrence of new conduction states is intimately linked to the topology of the surface and not limited to foams of elemental carbon. Our interpretation based on rehybridization theory indicates that conduction in the foam derives from first- and second-neighbor interactions between $p_{\parallel}$ orbitals lying in the surface plane, which are related to $p_{\perp}$ orbitals of graphene. The topologically protected conducting state occurs on bare and hydrogen-terminated foam surfaces and is thus unrelated to dangling bonds. Our results for carbon foam indicate that the conductance behavior may be further significantly modified by surface patterning.

DOI: 10.1103/PhysRevLett.112.026803 PACS numbers: 73.40.-c, 71.15.-m, 72.80.Vp, 73.22.Pr

There is growing interest in topologically complex carbon foam structures [1–8] that contain both sp^2 and sp^3 hybridized atoms. Most experimental studies have focussed on the synthesis and structural characterization of carbon foams [2–4] that are closely related to previously postulated structures [5,6,8]. Electronic properties of foams [1,5–7] have received much less attention than their structural stability in spite of the obvious possibility to fine-tune the fundamental band gap value in-between zero in sp^2-bonded graphene and 5.5 eV in sp^3-bonded diamond by modifying the foam morphology.

Here we report results of *ab initio* electronic structure and quantum conductance calculations indicating the emergence of conduction at the surface of semiconducting carbon foams. Occurrence of new conduction states in these systems is intimately linked to the topology of the surface and not limited to foams of elemental carbon. Our interpretation based on rehybridization theory indicates that conduction in the foam derives from first- and second-neighbor interactions between $p_{\parallel}$ orbitals lying in the surface plane, which are related to $p_{\perp}$ orbitals of graphene. The topologically protected conducting state occurs on bare and hydrogen-terminated foam surfaces and is thus unrelated to dangling bonds. Our results for carbon foam indicate that the conductance behavior may be further significantly modified by surface patterning.

The bulk carbon foam, depicted in Fig. 1(a), is a cellular structure resembling vaguely a fused triangular array of (6,0) zigzag nanotubes. In contrast to a nanotube array, the walls of the foam cells consist of 60% sp^2 bonded atoms shared by two neighboring cells and 40% sp^3 bonded atoms shared by three adjacent cells. Density-functional based tight-binding (DFTB) results indicate that the bulk structure is a semiconductor [6] with a band gap of 2.55 eV.

Cleavage normal to the long cell axis may generate two different surfaces. We distinguish the sp^3 surface terminated by C atoms, which were fourfold coordinated in the bulk, from the sp^2 surface terminated by atoms that were threefold coordinated. For computational reasons, we will represent the surface by slabs of finite thickness with two identical surfaces that are either bare or terminated by hydrogen. The optimum structure of the thinnest foam slab with sp^3 termination is shown in Fig. 1(b) and that of the thinnest sp^2-terminated slab in Fig. 1(c). We will focus on these thinnest slabs in the main manuscript and demonstrate

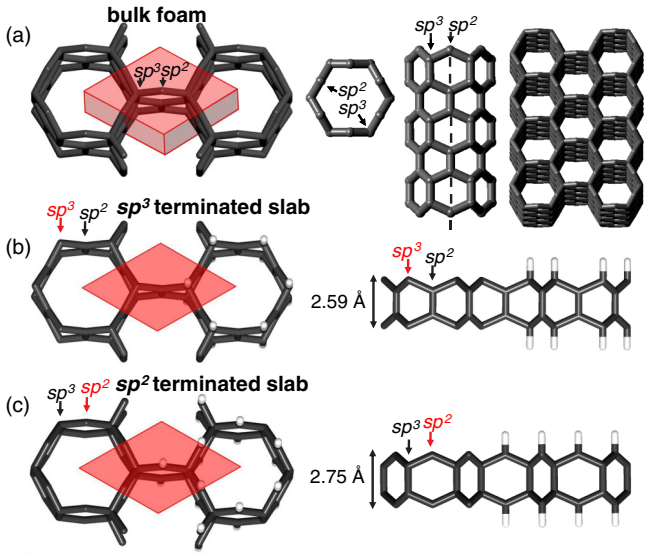

FIG. 1 (color online). Geometry of carbon foam and thin foam slabs. (a) Structure of bulk foam and that of an individual foam cell in side and top view, allowing us to distinguish sp^2 and sp^3 sites. The dashed line shows the long cell axis. The perspective view in the right panel depicts a larger bulk segment. Structure of (b) an sp^3-terminated and (c) an sp^2-terminated thin foam slab. The tilted view used in left panels depicts the structure and primitive unit cells. The right panels in (b) and (c) are side views of the structure that better illustrate the type of termination and illustrate partial hydrogen coverage.

the generality of our results for thicker slabs in the Supplemental Material [9].

Our numerical results for the equilibrium structure, stability and electronic properties of carbon foam slabs are based on density functional theory (DFT) as implemented in the SIESTA code [10]. The different foam surfaces are represented by a periodic array of slabs, separated by a 15 Å thick vacuum region. We used the Ceperley-Alder [11] exchange-correlation functional as parameterized by Perdew and Zunger [12], norm-conserving Troullier-Martins pseudopotentials [13], and a double-ζ basis including polarization orbitals. The reciprocal space was sampled by a fine grid [14] of $16 \times 16 \times 1$ k points in the Brillouin zone of the primitive surface unit cell. We used a mesh cutoff energy of 180 Ry to determine the self-consistent charge density, which provided us with a precision in total energy of $\lesssim 2$ meV/atom.

Transport properties of the slabs were investigated using the nonequilibrium Green's function (NEGF) approach as implemented in the TRAN-SIESTA code [15]. For structures optimized by DFT, we used a single-ζ basis with polarization orbitals, the same 180 Ry mesh cutoff energy, and a $8 \times 8 \times 1$ k-point grid [14].

Our DFT results for the band structure of the hydrogen-covered thin carbon slab with two sp^3 surfaces, shown in Fig. 1(b), are presented in Fig. 2(a). These results suggest this system to be semiconducting [16], same as its bulk counterpart [6]. On the other hand, the H-covered, sp^2-terminated slab, depicted in Fig. 1(c), is clearly metallic according to the band structure results in Fig. 2(b). This result is surprising, since conduction in semiconducting carbon structures including diamond has so far only been observed in presence of unsaturated dangling bonds [17]. Our band structure results in Fig. 2(b) also show a Dirac-like cone similar to graphene at the K point in the Brillouin zone. Moderate n doping should be able to align it with the Fermi level, providing carriers with the same desirable properties as graphene.

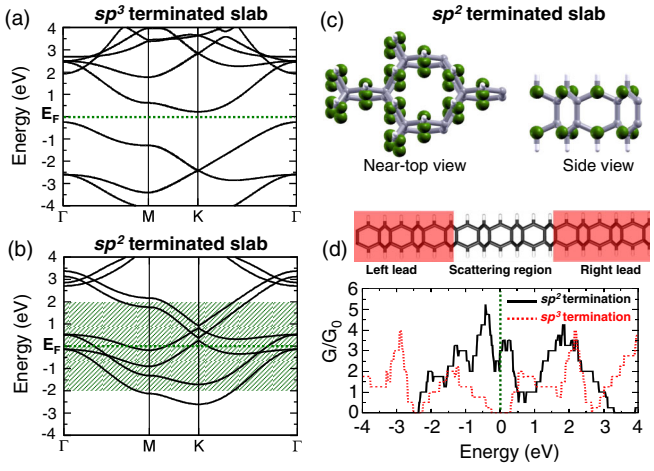

FIG. 2 (color online). Electronic structure of thin foam slabs. DFT-based band structure of a thin, hydrogen-covered foam slab with (a) sp^3 and (b) sp^2 termination on both sides. (c) Charge distribution in the sp^2-terminated slab corresponding to states in the energy range $E_F - 2$ eV $< E < E_F + 2$ eV, indicated by shading in (b). (d) Conductance G of sp^3- and sp^2-terminated slabs along the armchair direction, in units of the conduction quantum G_0.

To learn more about the character of the new conduction states, we display in Fig. 2(c) the charge density associated with states close to E_F, shown by the shaded region in Fig. 2(b). These states with $p_\parallel$ character, which are oriented within the surface plane of the foam, are located only on the sp^2 sublattice. This is very different from graphene, where conduction is caused by nearest-neighbor hopping between $p_\perp$ orbitals oriented normal to the surface, which are equally occupied at all lattice sites.

To judge the suitability of carbon foam for electronic applications, we calculated quantum conductance of hydrogen-covered thin sp^2- and sp^3-terminated carbon foam slabs, shown in Figs. 1(b)–(c), and present the results in Fig. 2(d). These results reflect our band structure results, namely a large conductance at small bias values in the sp^2-terminated carbon foam slab and a conduction gap of 0.6 eV in the sp^3-terminated slab. Additional results [9], also for thicker slabs, suggest that conduction is linked to the sp^2 termination of the carbon foam surface and nearly isotropic.

To confirm the generality of this finding and obtain insight into its origin, we used the linear combination of atomic orbitals (LCAO) technique [18–20] to study the electronic structure of carbon foam slabs [9]. Our results for the sp^2-terminated slab of interest are presented in Figs. 3(a)–(c). The band associated with conduction, obtained by considering only nearest-neighbor interactions and presented in Fig. 3(a), was found to be quite different from its DFT-based counterpart in Fig. 2(b). To find out if this difference is caused by omitting second and third neighbor interactions, we introduced these interactions in our initial Hamiltonian [9]. By selectively modifying individual hopping parameters, we have found that (i) the most significant changes in the electronic structure, including band broadening near E_F, are caused by second-neighbor $V_{pp\sigma}(2)$ and $V_{pp\pi}(2)$ interactions, (ii) $V_{ss\sigma}(2)$ and $V_{sp\sigma}(2)$ interactions between second neighbors do not affect the electronic structure near E_F and can be neglected, and (iii) third-neighbor interactions contribute very little to the electronic structure and can also be safely neglected. Results obtained using the Hamiltonian augmented by second-neighbor interactions between $p_\parallel$ states [9], presented in Fig. 3(b), agree much better with the DFT results of Fig. 2(b), in particular regarding the width of the occupied part of the conduction band.

The effect of the second-neighbor interaction is even more pronounced in the electronic structure of the bulk foam, shown in Figs. 3(d)–(f). As seen from the comparison

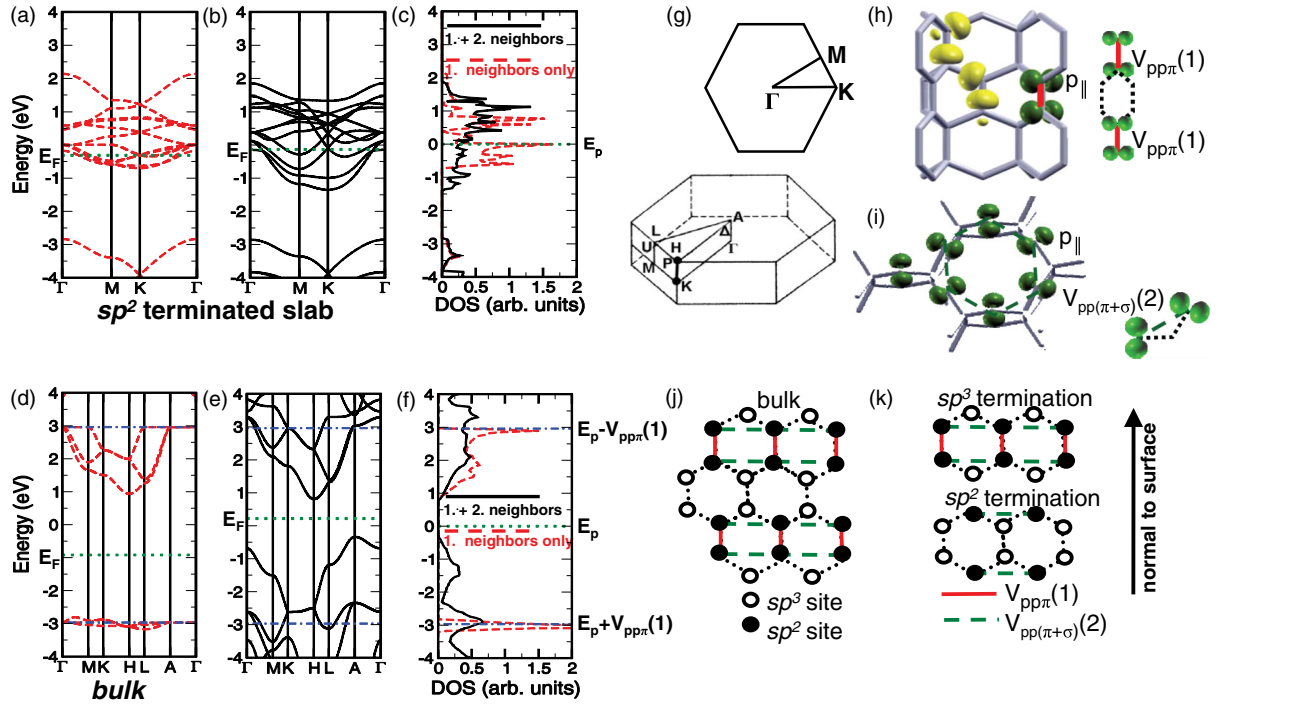

FIG. 3 (color online). Interpretation of electronic structure results for the sp^2-terminated slab (a)–(c) and bulk foam (d)–(f) using the LCAO technique. Band structure results considering only nearest-neighbor interaction [(a) and (d)], results of calculations that also include second-neighbor interaction between $p_\parallel$ states [(b) and (e)], and the corresponding densities of states [(c) and (f)]. (g) High-symmetry points in the slab and bulk Brillouin zones. (h) Rehybridized orbitals used in the calculation. $p_\parallel$ orbitals, shown in darker (green) shade, are responsible for conduction. (i) Tilted top view of the second neighbor-interaction between $p_\parallel$ states that dominate band dispersion near E_F. Connectivity diagram for the bulk (j) and thin foam slabs (k) that helps explain the semiconducting behavior of bulk and sp^3-terminated foam, and the origin of the conducting state at the sp^2-terminated surface.

between Figs. 3(d) and 3(e), neglecting the second-neighbor interaction in Fig. 3(d) caused a drastic narrowing of the bulk valence band and a significant increase in the fundamental band gap. LCAO calculations for the bulk with both first- and second-neighbor interactions, presented in Fig. 3(e), indicate an indirect A-H fundamental band gap of $E_g = 1.12$ eV, in qualitative agreement with non-self-consistent DFTB results.

Having shown that the electronic structure near the Fermi level is well reproduced by the LCAO Hamiltonian, which also considers second-neighbor interactions between p states, we proceed to identify the reason for the fundamental difference between the sp^2-terminated metallic and sp^3-terminated semiconducting slab. We use the rehybridization theory[21,22] to identify proper hybrid orbitals, since the atomic arrangements in the foam are generally not purely linear, hexagonal or tetrahedral. Hybrid orbitals $|h_i\rangle$ with $i = 1, 2, 3, 4$, which are associated with an atom, are linear combinations of the $|s\rangle$ and a $|p\rangle$ atomic orbital at this site. The direction of the $|p\rangle$ orbital is not that of the Cartesian axes, but rather taken as that of nearest-neighbor bonds to up to three neighbors. The relative weights of the atomic orbitals are constructed [23] by enforcing the orthogonality condition $\langle h_i|h_j\rangle = \delta_{ij}$. This orthogonality condition is also used to construct any remaining hybrid orbitals. Selected hybrids at fourfold coordinated sp^3 sites and at threefold coordinated sp^2 sites are shown in Fig. 3(h).

Analysis of the foam eigenstates at E_F indicates dominance of $p_\parallel$ hybrids, highlighted by the darker color Fig. 3(h), at sp^2 sites only. While parallel to the slab surface, these $p_\parallel$ orbitals are not aligned along a spatially fixed direction, but rather are locally normal to the graphitic strips lining the foam cells. These $p_\parallel$ hybrids on the sp^2 sublattice play the role of π orbitals in the Hückel Hamiltonian that describes most of the interesting physics in this system. We will show below that considering only first- and second-neighbor interaction in the Hückel Hamiltonian is sufficient to explain, why bulk foam and sp^3-terminated slabs are semiconducting, whereas sp^2-terminated slabs become metallic.

The spatial distribution of the $p_\parallel$-dominated states at E_F at one of the slab surfaces, shown in Fig. 3(i), agrees well with the DFT results presented in Fig. 2(c). In a Hückel Hamiltonian with up to second-neighbor interactions, the $p_\parallel$ hybrids may interact in two ways only. The first type of interaction is normal to the surface and involves pairs of adjacent sp^2 sites, which interact by the first-neighbor $V_{pp\pi}(1)$ interaction. This is shown schematically by the red solid lines in the right panel of Fig. 3(h) and in

Figs. 3(j)–(k), which represent the connectivity diagram of the foam. The second type of interaction is in-plane and much weaker, involving only the second-neighbor $V_{pp\pi}(2)$ and $V_{pp\sigma}(2)$ interactions between $p_\parallel$ states. This is shown schematically by the green dashed lines in the right panel of Fig. 3(i) and in Figs. 3(j)–(k). In contrast to graphene, where the relatively strong $V_{pp\pi}(1)$ interaction forms a network that connects all atoms in the layer, this interaction connects only pairs of adjacent sp^2 sites in the carbon foam, as illustrated in Figs. 3(j)–(k).

We conclude that bulk foam states near E_F resemble those of a set of carbon dimers, where the $V_{pp\pi}(1)$ interaction splits the E_p energy eigenvalue into $E_p \pm V_{pp\pi}(1)$, indicated by the blue dash-dotted lines in Figs. 3(d)–(f). This corresponds to opening up a large fundamental band gap with $E_g = 2|V_{pp\pi}(1)|$, which turns carbon foam to a semiconductor. The δ-function-like localized states at $E_p \pm V_{pp\pi}(1)$, originating from decoupled dimers, are clearly visible in the density of states of the system with nearest-neighbor interactions only, shown by the red dashed line in Fig. 3(f). Much weaker second-neighbor $V_{pp\pi}(2)$ and $V_{pp\sigma}(2)$ interactions couple these dimers and broaden the localized states into wide valence and conduction bands, shown by the solid black lines in the density of states in Fig. 3(f).

Now it is rather straightforward to explain the fundamental difference between the bulk, sp^3- and sp^2-terminated surfaces in terms of conductivity. Deciding whether a structure is metallic or semiconducting boils down to the simple question, whether *all* of the sp^2 sites are connected as first neighbors to another sp^2 site. If so, then all energy eigenvalues E_p of the $p_\parallel$ states will split by $V_{pp\pi}(1)$ into the eigenvalue pair $E_p \pm V_{pp\pi}(1)$, which opens up a gap. This is the case for the bulk and an sp^3-terminated surface of the foam. If, on the other hand, there are at least *some* sp^2 sites present with no first-neighbor bonds to other sp^2 sites, then the energy eigenvalue E_p of these $p_\parallel$ states will not split. Presence of partly filled $p_\parallel$ states at $E_p = E_F$ indicates that such a system should be conducting. The second-neighbor interaction between $p_\parallel$ states provides a weak coupling between sp^2 site pairs or lone sp^2 sites at the surface, as shown schematically in Figs. 3(j) and 3(k). In the bulk or in the sp^3-terminated foam, this second-neighbor interaction broadens the pair of sharp eigenvalues into a valence and conduction band that are still separated by a band gap, keeping their semiconducting character. At the sp^2-terminated surface, the weak second-neighbor interaction between $p_\parallel$ states at sp^2 sites with no sp^2 nearest neighbors will broaden the state at E_p to a metallic band, as seen also in the density of states presented in Fig. 3(c). This behavior is not restricted to carbon foam, but should also occur at surfaces of isomorphic foams of Si, Si-carbides, or BN systems [24].

This reasoning also explains, why conductance depends only on the presence of sp^2 sites with a particular topological arrangement. We may thus conclude that the conducting state at sp^2-terminated surfaces is topologically protected and is independent of the fact that the surface has been represented by a finite-thickness slab. This finding is furthermore confirmed by our electronic structure and conductance results for a thicker slab [9]. With increasing thickness, the electronic structure of finite slabs approaches that of the bulk material [16].

Our conclusions regarding occurrence of states at E_F are valid not only for perfect sp^2-terminated surfaces, but also for all defective structures that contain sp^2 sites with no sp^2 nearest neighbors. Isolated monatomic vacancies in the bulk will produce corresponding midgap defect states. Lithographic patterning of the sp^3-terminated semiconducting surface by selective removal of lines of surface atoms will yield lines with sp^2 termination that will behave as conductive nanowires.

In conclusion, we have identified theoretically an unusual conduction mechanism occurring at the sp^2-terminated surface of a semiconducting carbon foam. To obtain microscopic insight into the origin of this mechanism, we augmented *ab initio* electronic structure and quantum conductance calculations by rehybridization theory calculations. We found that the occurrence of new conduction states in this system is intimately linked to the topology of the surface and not limited to foams of elemental carbon. Our interpretation based on rehybridization theory indicates that conduction in the foam derives from first- and second-neighbor interactions between $p_\parallel$ orbitals lying in the surface plane, which are related to $p_\perp$ orbitals of graphene. The topologically protected conducting state occurs on bare and hydrogen-terminated foam surfaces and is thus unrelated to dangling bonds. Our results for carbon foam indicate that the conductance behavior may be further significantly modified by surface patterning, allowing us to create conductive paths at the surface of the semiconducting foam matrix.

This study was supported by the National Science Foundation Cooperative Agreement No. #EEC-0832785, titled "NSEC: Center for High-Rate Nanomanufacturing." Computational resources have been provided by the Michigan State University High Performance Computing Center.

*tomanek@pa.msu.edu

[1] H. Wang, K. Sun, F. Tao, D. J. Stacchiola, and Y. H. Hu, Angew. Chem., Int. Ed. Engl. **52**, 9210 (2013).

[2] Y. Zhu, S. Murali, M. D. Stoller, K. J. Ganesh, W. Cai, P. J. Ferreira, A. Pirkle, R. M. Wallace, K. A. Cychosz, M. Thommes, D. Su, E. A. Stach, and R. S. Ruoff, Science **332**, 1537 (2011).

[3] D. P. Hashim, N. T. Narayanan, J. M. Romo-Herrera, D. A. Cullen, M. G. Hahm, P. Lezzi, J. R. Suttle, D. Kelkhoff, E. Muñoz Sandoval, S. Ganguli, A. K. Roy, D. J. Smith,

R. Vajtai, B. G. Sumpter, V. Meunier, H. Terrones, M. Terrones, and P. M. Ajayan, Sci. Rep. **2**, 363 (2012).
[4] Z. Chen, W. Ren, L. Gao, B. Liu, S. Pei, and H.-M. Cheng, Nat. Mater. **10**, 424 (2011).
[5] K. Umemoto, S. Saito, S. Berber, and D. Tománek, Phys. Rev. B **64**, 193409 (2001).
[6] A. Kuc and G. Seifert, Phys. Rev. B **74**, 214104 (2006).
[7] X. Jiang, J. Zhao, Y.-L. Li, and R. Ahuja, Adv. Funct. Mater. **23**, 5846 (2013).
[8] Z. Zhu and D. Tománek, Phys. Rev. Lett. **109**, 135501 (2012).
[9] See Supplemental Material at http://link.aps.org/supplemental/10.1103/PhysRevLett.112.026803 for calculations addressing thicker slabs, reliability of our band structure calculations, and the construction of the LCAO Hamiltonian.
[10] E. Artacho, E. Anglada, O. Dieguez, J. D. Gale, A. Garcia, J. Junquera, R. M. Martin, P. Ordejon, J. M. Pruneda, D. Sanchez-Portal, and J. M. Soler, J. Phys. Condens. Matter **20**, 064208 (2008).
[11] D. M. Ceperley and B. J. Alder, Phys. Rev. Lett. **45**, 566 (1980).
[12] J. P. Perdew and A. Zunger, Phys. Rev. B **23**, 5048 (1981).
[13] N. Troullier and J. L. Martins, Phys. Rev. B **43**, 1993 (1991).
[14] H. J. Monkhorst and J. D. Pack, Phys. Rev. B **13**, 5188 (1976).
[15] M. Brandbyge, J.-L. Mozos, P. Ordejón, J. Taylor, and K. Stokbro, Phys. Rev. B **65**, 165401 (2002).
[16] Limitations of DFT results regarding band gaps are discussed in the Supplemental Material [9].
[17] J. Sone and S. Okada, J. Phys. Soc. Jpn. **82**, 064706 (2013).
[18] J. C. Slater and G. F. Koster, Phys. Rev. **94**, 1498 (1954).
[19] D. Tomanek and M. A. Schluter, Phys. Rev. Lett. **67**, 2331 (1991).
[20] D. A. Papaconstantopoulos, *Handbook of the Band Structure of Elemental Solids* (Plenum Press, New York, 1986).
[21] R. C. Haddon, J. Am. Chem. Soc. **108**, 2837 (1986).
[22] R. C. Haddon and L. T. Scott, Pure Appl. Chem. **58**, 137 (1986).
[23] Z. G. Fthenakis, R. W. A. Havenith, M. Menon, and P. W. Fowler, Phys. Rev. B **75**, 155435 (2007).
[24] Whereas carbon foam is less stable than graphene, the foam structure of silicon is more stable than silicene.